FiMAP: A Fast Identity-by-Descent Mapping Test for Biobank-scale Cohorts

Han Chen[1,2,*], Ardalan Naseri[2], Degui Zhi[1,2,*]

[1] Human Genetics Center, Department of Epidemiology, Human Genetics and Environmental Sciences, School of Public Health, The University of Texas Health Science Center at Houston, Houston, Texas 77030, USA.

[2] Center for Precision Health, School of Biomedical Informatics, The University of Texas Health Science Center at Houston, Houston, Texas 77030, USA.

[*] Correspondence: Han.Chen@uth.tmc.edu, Degui.Zhi@uth.tmc.edu

Abstract

Although genome-wide association studies (GWAS) have identified tens of thousands of genetic loci, the genetic architecture is still not fully understood for many complex traits. Most GWAS and sequencing association studies have focused on single nucleotide polymorphisms or copy number variations, including common and rare genetic variants. However, phased haplotype information is often ignored in GWAS or variant set tests for rare variants. Here we leverage the identity-by-descent (IBD) segments inferred from a random projection-based IBD detection algorithm in the mapping of genetic associations with complex traits, to develop a computationally efficient statistical test for IBD mapping in biobank-scale cohorts. We used sparse linear algebra and random matrix algorithms to speed up the computation, and a genome-wide IBD mapping scan of more than 400,000 samples finished within a few hours. Simulation studies showed that our new method had well-controlled type I error rates under the null hypothesis of no genetic association in large biobank-scale cohorts, and outperformed traditional GWAS approaches and variant set tests when the causal variants were untyped and rare, or in the presence of haplotype effects. We also applied our method to IBD mapping of six anthropometric traits using the UK Biobank data and identified a 4 cM region on chromosome 8 associated with multiple traits related to body fat distribution or weight.

Keywords: identity-by-descent, association mapping, linkage, biobank, variance component model

Introduction

Identity-by-descent (IBD) segments between two individuals are inherited from their common ancestor, without recombination.[1] They have been widely used in forensic genetics,[2, 3] as well as population genetics to detect evidence of natural selection, and to estimate the demographic history such as bottlenecks and admixture.[4-6] In a genome-wide association study (GWAS) with cryptically related samples, the average proportion of the genome shared IBD can be used to infer the degree of relatedness,[1, 7] and to construct an empirical kinship matrix to account for cryptic relatedness in GWAS.[8-11]

IBD mapping is the study of association between the sharing of IBD segments and phenotypic similarities. Early IBD mapping studies were mostly in linkage analysis for family studies.[12-15] IBD mapping methods for other study designs have also been developed, such as those searching for chromosome segments shared by distantly related patients,[16] testing for association with haplotype clusters,[17] and comparing pairwise IBD rates in case-case and case-control pairs.[18] Indeed, IBD mapping has successfully identified genomic regions associated with Parkinson's disease,[19] serum triglycerides,[20] multiple sclerosis,[21] and amyotrophic lateral sclerosis.[22]

Although IBD mapping is not yet a widely-applied method, it holds promise to uncover untyped rare variant and haplotypic effects, that are still escaping the search of the "missing heritability". While most common variants are tagged by genotypes from arrays and can be well-imputed, rare variants are still not well covered. IBD mapping can indirectly test the effects of rare variants co-segregated with the IBD segments and recover the association signal. Further, the combination of multiple variants on an IBD segment, each individually weakly associated with the phenotype and thus difficult to be identified by single variant association tests, can be captured by IBD mapping. As the phase information is often ignored in traditional GWAS approaches and variant set tests for rare genetic variants,[23-29] IBD mapping leverages such

information and is less susceptible to genotyping or sequencing errors. It can better identify association signals from rare variants and haplotype effects,[18] and therefore offers a unique angle to investigate genetic associations.

While promising, IBD mapping were not popular due to several technical challenges. First, IBD mapping requires accurate phasing of haplotypes. This difficulty is mostly addressed by current phasing software.[30-32] Second, the power of IBD mapping methods is linked with the number of IBD segments in the sample. While the density of IBD segments in families and inbred populations are high, their density in outbred populations can be much lower. Nonetheless, with the availabilities of large biobanks, the sample sizes are large enough to harbor a large number of IBD segments. For example, our recent studies found that each haplotype of a UK Biobank participant is covered by about 10 5cM IBD segments shared with other UK Biobank participants.[33] Third, traditional IBD segment calling methods are not efficient and cannot scale up to modern biobank-scale cohorts with hundreds of thousands of samples. Fortunately, this challenge is largely resolved by a new generation of efficient IBD segment detection methods, either based on the positional Burrows Wheeler transform (PBWT) algorithm,[34] such as RaPID,[35] hap-IBD,[36] and TPBWT,[37] or based on advanced string hashing such as FastSMC[38] and iLASH.[39] These methods typically achieve $O(N)$ complexity, where N is the sample size, and have made IBD segment calling computationally feasible in biobank-scale cohorts with hundreds of thousands to millions of individuals. However, even with the advancements of abovementioned technologies, existing IBD mapping methods are still not scalable to large sample sizes due to lack of efficient statistical tests for IBD mapping.

To address the main computational challenge for biobank-scale cohorts that any IBD mapping methods with $O(N^2)$ computational time complexity or higher would quickly become infeasible, we have developed FiMAP, a fast IBD mapping test for biobank-scale cohorts. FiMAP leverages IBD segments identified by RaPID[35] and constructs a genotype similarity tensor on the whole

genome (**Figure 1**). The genotype similarity tensor is a collection of $N \times N$ pairwise local IBD matrices that change across the whole genome. Each local IBD matrix is a sparse matrix indicating the proportion of IBD sharing between any two individuals in the given genomic region, with most elements being 0. The average of local IBD matrices across the whole genome is the global IBD matrix representing the average proportion of IBD sharing, which can be used as a kinship coefficient matrix to account for genetic relatedness in the study samples. FiMAP leverages a random matrix-based algorithm to speed up the computation, so that a genome-wide IBD mapping analysis for hundreds of thousands of study samples can be finished within a few hours. We also demonstrate the application of FiMAP to the IBD mapping analysis of six anthropometric traits in the UK Biobank.

Methods

Variance component models

Variance component models have long been used in linkage analysis to identify genetic loci linked with quantitative traits.[12-15] Consider a linear mixed model $Y_i = X_i\beta + b_i + \delta_{il} + \varepsilon_i$ for individual i, where Y_i is the phenotype, X_i are c fixed-effect covariates with effect sizes β, b_i is the polygenic random effect accounting for global relatedness, δ_{il} is the random effect of local relatedness at genetic locus l, we stack N individuals to get length N vectors Y, b, δ_l, ε, and an $N \times c$ matrix X, from Y_i, b_i, δ_{il}, ε_i, X_i, respectively. The vector $b \sim N(0, \sigma_G^2\Phi)$ are the random effects for the $N \times N$ global IBD (or kinship) matrix Φ denoting the average proportion of IBD sharing between any two individuals, $\delta_l \sim N(0, \sigma_l^2\Psi_l)$ are the random effects for the $N \times N$ local IBD matrix Ψ_l at this genetic locus l, and ε are independent and identically distributed errors that follow a normal distribution with mean 0 and variance σ_E^2. Under the null hypothesis of no association with the

quantitative trait at genetic locus l, the random effects δ_l are equal to 0 and this is equivalent to testing variance component hypotheses $H_0: \sigma_l^2 = 0$ vs $H_1: \sigma_l^2 > 0$.

<u>The asymptotic test</u>

Let $\hat{\Sigma} = \hat{\sigma}_E^2 I_N + \hat{\sigma}_G^2 \Phi$, where both $\hat{\sigma}_E^2$ and $\hat{\sigma}_G^2$ are estimated from the null model (with $\delta_l = 0$) in the matrix-vector form $Y = X\beta + b + \varepsilon$. Let $r = Y - X\hat{\beta} - \hat{b}$ be the length N residual vector, where both $\hat{\beta}$ and $\hat{b}$ are estimated from this null model, the classical score-type variance component test $Q_l = \frac{1}{\hat{\sigma}_E^4} r^T \Psi_l r$ asymptotically follows a chi-square mixture distribution $\sum_j \zeta_j \chi_{1,j}{}^2$,[27, 40, 41] where $\chi_{1,j}{}^2$ are independent chi-square distributions with 1 degree of freedom, and ζ_j's are the eigenvalues of $\hat{P}^{\frac{1}{2}} \Psi_l \hat{P}^{\frac{1}{2}}$, where $\hat{P} = \hat{\Sigma}^{-1} - \hat{\Sigma}^{-1} X (X^T \hat{\Sigma}^{-1} X)^{-1} X^T \hat{\Sigma}^{-1}$ is the $N \times N$ projection matrix.[42]

<u>The finite-sample adjustment</u>

Although under regularity conditions, $\hat{\sigma}_E^2$ and $\hat{\sigma}_G^2$ are consistent estimators for variance component parameters σ_E^2 and σ_G^2 under the null hypothesis $H_0: \sigma_l^2 = 0$, the classical score-type variance component test above treats them as fixed numbers and ignores the variability in their estimation, which could result in not well-calibrated p values in finite samples. This is a known issue for score-type variance component tests in microbiome association studies with small sample sizes.[43-45] Despite large sample sizes in biobank-scale cohorts, the local IBD matrix Ψ_l for genetic locus l is often sparse, which could invalidate asymptotic inference on the quadratic form $Q_l = \frac{1}{\hat{\sigma}_E^4} r^T \Psi_l r$. We note that $\hat{\Sigma}^{-1}(Y - X\hat{\beta}) = \hat{\sigma}_E^{-2} r$, and $\hat{\sigma}_E^2 = \frac{(Y - X\hat{\beta})^T (\frac{\hat{\Sigma}}{\hat{\sigma}_E^2})^{-1} (Y - X\hat{\beta})}{N - c} = \frac{r^T \hat{\Sigma} r}{\hat{\sigma}_E^2 (N - c)}$, where $\frac{\hat{\Sigma}}{\hat{\sigma}_E^2}$ is free of σ_E^2. To account for the variability in estimating σ_E^2, we can rewrite $Q_l = (N - c) \frac{r^T \Psi_l r}{r^T \hat{\Sigma} r}$, and compute the finite-sample p-value as $P(\sum_j \xi_j \chi_{1,j}{}^2 > 0)$, where ξ_j's are the eigenvalues of $\hat{P}^{\frac{1}{2}} (\Psi_l - \frac{Q_l}{N - c} \hat{\Sigma}) \hat{P}^{\frac{1}{2}}$.

<u>FiMAP</u>

As both $\hat{P}$ and Ψ_l are $N \times N$ matrices (and $\hat{P}$ is not sparse), conducting the classical score-type variance component test, without or with the finite-sample adjustment, requires $O(N^2)$ memory footprint and $O(N^3)$ computational time complexity, which becomes infeasible for hundreds of thousands to millions of individuals. To solve this computational challenge, we use an $N \times B$ random matrix R to compute approximated top B eigenvalues of $\hat{P}^{\frac{1}{2}}\Psi_l\hat{P}^{\frac{1}{2}}$ from $\frac{1}{B}R^T\Psi_l R$. Specifically, we start with a Cholesky decomposition of the sparse global IBD matrix $\Phi = LL^T$, then simulate length N random vectors r_1 and r_2 from a standard normal distribution to compute $r_3 = \hat{\sigma}_E r_1 + \hat{\sigma}_G L r_2$ and $r_4 = \hat{\Sigma}^{-1}r_3 - \hat{\Sigma}^{-1}X(X^T\hat{\Sigma}^{-1}X)^{-1}X^T\hat{\Sigma}^{-1}r_3$. Therefore, we have $r_4 \sim N(0, \hat{P})$ and repeat the process B times to get an $N \times B$ random matrix R. Assuming both the global IBD matrix Φ and the local IBD matrices Ψ_l are block-diagonal (with a bounded largest block size) and sparse, then both L and $\hat{\Sigma}^{-1}$ are also block-diagonal, and r_3 and r_4 do not require any matrix-vector multiplications involving full dense $N \times N$ matrices. If both the largest block size and B are $O(1)$, then the overall computational complexity of FiMAP is $O(N)$. Moreover, for the finite-sample adjustment, we can pre-compute $\frac{1}{B}R^T\hat{\Sigma}R$ only once in a genome-wide scan, and approximate top B eigenvalues of $\hat{P}^{\frac{1}{2}}(\Psi_l - \frac{Q_l}{N-c}\hat{\Sigma})\hat{P}^{\frac{1}{2}}$ by $\frac{1}{B}R^T\Psi_l R - \frac{Q_l}{(N-c)B}R^T\hat{\Sigma}R$.

In reality, we observe the start and end positions of each IBD segment between two individuals (e.g., from RaPID[35]). Therefore, for a genetic locus l, instead of a local IBD matrix Ψ_l with 2 identical chromosomes for each individual with themselves, we construct $\widetilde{\Psi}_l = \Psi_l - 2I_N$, with each element denoting the proportion of IBD segments between two individuals in the given region. For biobank-scale cohorts, $\widetilde{\Psi}_l$ is highly sparse with most elements 0. Assuming a total of L equally spaced genomic regions across the whole genome, the global IBD matrix $\Phi = \frac{1}{L}\sum_{l=1}^{L}\widetilde{\Psi}_l + 2I_N$ is the average of the local IBD matrices Ψ_l's. In our implementation, we pre-compute an offset $A = 2R^TR - \frac{2r^Tr}{N-c}R^T\hat{\Sigma}R$ only once in a genome-wide scan. For each genetic

locus l, we then compute the finite-sample p-value as $P(\sum_j \tilde{\xi}_j \chi_{1,j}{}^2 > 0)$, where $\tilde{\xi}_j$'s are the eigenvalues of $\frac{1}{B}\left\{A + R^T\widetilde{\Psi}_l R - \frac{r^T\widetilde{\Psi}_l r}{N-c} R^T\hat{\Sigma}R\right\}$. Note that $\frac{1}{B}R^T\hat{\Sigma}R$ is also pre-computed, for each genetic locus l with observed IBD proportion matrix $\widetilde{\Psi}_l$, we only need to update the $B \times B$ matrix $R^T\widetilde{\Psi}_l R$ and the scalar $r^T\widetilde{\Psi}_l r$.

<u>Simulation studies</u>

We used RaPID IBD segment calls from the UK Biobank array-typed genotype data to simulate phenotype data, and evaluated type I error rates and power of FiMAP in identifying genetic associations. Specifically, we used RaPID IBD segment calls on all 22 autosomes to construct the global IBD matrix Φ for 487,279 individuals. For individuals with no inbreeding, the diagonal elements of Φ is equal to 2, which is 4 times the theoretical kinship coefficient, indicating the total length of IBD segments shared by each individual with themselves is twice the total length of all autosomes. The off-diagonal elements of Φ are the total length of IBD segments shared by each pair of individuals, divided by the total length of all autosomes. To ensure the sparsity of the global IBD matrix Φ, we set off-diagonal elements less than 0.088 to 0, which is equivalent to including fourth-degree relatives or closer in the kinship matrix (kinship coefficient ≥ 0.022). We then chunked 22 autosomes into 1 cM windows and assembled 3,403 local IBD matrices by computing the proportion of IBD sharing between each pair of individuals in each 1 cM window (the last window on each chromosome is shorter than 1 cM). We set the number of random vectors used in FiMAP $B = 100$ in all simulation studies.

In type I error simulations, we randomly selected 400,000 individuals and subset the global IBD matrix Φ to get a submatrix Φ_0. We then simulated age from a normal distribution with mean 50 and standard deviation 5, and sex from a Bernoulli distribution with probability 0.5. A continuous phenotype Y_i for individual i was simulated as $Y_i = 0.05age_i + 0.5sex_i + b_i + \varepsilon_i$, where the vector form b followed a multivariate normal distribution with mean 0 and covariance matrix Φ_0,

and ε_i followed a standard normal distribution. Then we tested for the association with 3,403 local IBD matrices after adjusting for age and sex. We simulated 50 phenotype replicates and obtained a total of 170,150 p values under the null hypothesis of no local IBD random effects.

We also conducted power simulations to benchmark finite-sample FiMAP results with standard GWAS results as well as variant set tests, including the burden test,[26] SKAT,[27] SKAT-O,[28] and SMMAT[46] on the same 1 cM window. Using a random sample of N = 400,000 individuals from the UK Biobank, we simulated untyped ultra-rare causal variants that were not included in any of the tests for a fair comparison. Specifically, in each simulation replicate, we randomly selected a 1 cM window with at least 2 ultra-rare variants with MAF < 0.02%, we then assumed that all J ultra-rare variants with MAF < 0.05% in this window were causal variants and simulated a continuous phenotype Y_i for individual i as $Y_i = 0.05age_i + 0.5sex_i + \sum_{j=1}^{J} G_{ij}\beta_j + b_i + \varepsilon_i$, where age_i, sex_i, b_i and ε_i were simulated using the same parameter settings as in the type I error simulations, and the causal variant effect $\beta_j = \sqrt{\frac{0.005}{2MAF_j(1-MAF_j)}}$. Finite-sample FiMAP with local IBD matrices constructed from RaPID IBD segments called with length ≥ 3 cM, 5 cM, 10 cM were conducted. Using the directly genotyped data, we excluded variants with missing rate > 5% or MAF < 1% to mask the ultra-rare causal variants, and conducted a standard single-variant test commonly used in GWAS. We selected the minimum single-variant test p value in the same 1 cM window and applied a Bonferroni correction to account for multiple testing. We also conducted four variant set tests on the same genotyped data as used in the single-variant test, in the same 1 cM window: the burden test, SKAT, SKAT-O and SMMAT, all using the same Wu weights.[27] Empirical power was estimated as the proportion of p values (for the single-variant test, Bonferroni-corrected p values) less than 0.05 over 1,000 simulation replicates.

In addition, we simulated haplotype effects and compared FiMAP with IBD segments called with length ≥ 3 cM, 5 cM, 10 cM with the single-variant test as well as the aforementioned four

variant set tests. We computed all haplotypes between 68 and 72 cM on chromosome 8, with length ≥ 1 cM shared by 500 or more individuals from the UK Biobank using a PBWT-block algorithm.[47] In each simulation replicate, we used a random sample of N = 400,000 individuals and randomly sampled a causal haplotype. We simulated a continuous phenotype Y_i for individual i as $Y_i = 0.05age_i + 0.5sex_i + H_i\gamma + b_i + \varepsilon_i$, where age_i, sex_i, b_i and ε_i were simulated using the same parameter settings as in the type I error simulations, and H_i was the number of causal haplotypes carried by individual i, with possible values 0, 1, 2. The causal haplotype effect was assigned as $\gamma = \sqrt{\frac{0.005}{Var(H_i)}}$. We then tested the 1 cM window with the largest overlap with the causal haplotype using FiMAP, single-variant test and variant set tests.

<u>UK Biobank anthropometric traits</u>

We applied FiMAP to 6 anthropometric traits: waist circumference (N = 407,889), hip circumference (N = 407,844), standing height (N = 407,698), sitting height (N = 407,340), body mass index (N = 407,272), and body weight (N = 407,417), from the UK Biobank white British study participants with genetic ethnic group in Caucasians, after excluding individuals with inconsistent gender and biological sex. Each trait was adjusted for age, age^2, sex, their interactions, and top 10 ancestral principal components (PCs), and the residuals were rank normalized and analyzed using a linear mixed model with the same aforementioned fixed-effects covariates[48] and the global IBD matrix to model the covariance structure of the random intercept. We used RaPID IBD segment calls with length ≥ 5cM, and defined genomic regions l using 1 cM windows as used in our simulation studies, with a total of 3,403 test regions on 22 autosomes. We set the number of random vectors used in FiMAP $B = 100$ in all UK Biobank data analyses. For each trait, genome-wide significance was defined as finite-sample FiMAP p value < 0.05/3,403 = 1.47×10^{-5}, the Bonferroni-corrected threshold for 3,403 tests.

We also analyzed the same anthropometric traits in a GWAS setting using GMMAT[42] on imputed genetic variants with MAF ≥ 0.01%, imputation quality score ≥ 0.3, and missing rate < 5%. For each trait, genome-wide significance was defined as single-variant test p value $< 5 \times 10^{-8}$. In the conditional analysis, for each 1 cM window with a significant finite-sample FiMAP p value $< 1.47 \times 10^{-5}$, we performed stepwise model selection to identify a set of imputed genetic variants with GWAS p values that reached genome-wide significance in the ± 1 cM flanking regions (total length 3 cM) after conditioning on each other, and then adjusted for this set of imputed genetic variants in the conditional FiMAP analysis.

Results

Type I error rates

We first counted the numbers of non-zero off-diagonal elements in each of the 3,403 local IBD matrices for 1 cM windows, with sample size N = 487,279. The local IBD matrices were constructed from RaPID IBD segments called with length ≥ 3 cM, 5 cM, 10 cM. **Figure 2** shows that the number of non-zero off-diagonal elements increased as the IBD length cutoff decreased from 10 cM, 5 cM to 3 cM. For example, when the IBD length cutoff was 5 cM, the median number of non-zero elements per individual in local IBD matrices from the full sample was 17.5, with a range of 2.1 to 44.8. In contrast, in a random subset of N = 1,000 individuals, the median number of non-zero elements per individual was 0.037, with a range of 0.008 to 0.093. In the full sample, the maximum number of non-zero elements per individual in local IBD matrices with the IBD length cutoff of 3 cM was 468× the sample size, suggesting that the number of non-zero elements in any local IBD matrix at a given length cutoff (≥ 3 cM, 5 cM, or 10 cM) in the UK Biobank data was about a constant factor of N, thus the computational efficiency of FiMAP was guaranteed. On a computing server with dual Intel® Xeon® E5-2687W v4 CPU (3.00 GHz, 24

cores in total), analysis of each simulation replicate with N = 400,000 took about 206 minutes for IBD length cutoff 3 cM, 77 minutes for 5 cM, and 34 minutes for 10 cM, using 40 threads in parallel.

Asymptotic and finite-sample FiMAP p values under the null hypothesis of no local IBD random effects were shown in **Figure 3**. Asymptotic FiMAP p values were extremely conservative in the tail, while FiMAP p values with the finite-sample adjustment were well-calibrated. The median finite-sample FiMAP p value showed genomic inflation factors very close to 1 for IBD segments called with length ≥ 3 cM, 5 cM, 10 cM, suggesting that FiMAP with the finite-sample adjustment is a fast and valid IBD mapping test in large samples.

Power

As asymptotic FiMAP p values were extremely conservative in the tail from the type I error simulation studies, we only computed finite-sample FiMAP p values in the power simulation studies as well as the UK Biobank real data analysis. Assuming the causal variants in a 1 cM window were ultra-rare (with MAF < 0.05%) and not directly observed, **Figure 4A** shows that FiMAP with IBD segments called with length ≥ 3 cM and 5 cM outperformed the single-variant test (which was widely used in GWAS) and commonly used variant set tests. Of note, the single-variant test power, even with a Bonferroni correction that multiplied the minimum p value by the number of genotyped variants in the 1 cM window, was higher than the variant set tests with Wu weights[27] that favored variants with a lower MAF, suggesting that variant set tests may not perform well in the presence of a large number of neutral variants which could dilute the association signal. FiMAP with IBD segments called with length ≥ 10 cM had comparable performance with the variant set tests SKAT, SKAT-O and SMMAT.

In the presence of causal haplotype effects, FiMAP with IBD segments called with length ≥ 3 cM had the best power, followed by the single-variant test and FiMAP with IBD segments called

with length ≥ 5 cM (**Figure 4B**). FiMAP with IBD segments called with length ≥ 10 cM suffered from a substantial power loss, likely due to the fact that many shorter IBD segments tagging the causal haplotype in the region were not included.

UK Biobank anthropometric traits

For each anthropometric trait from the UK Biobank, the FiMAP analysis using the IBD length cutoff 5 cM took 48 CPU hours with a maximum memory footprint scaling linearly with the number of nonzero entries in the local IBD matrix Ψ_l. Each thread took less than 16 GB peak memory. As a comparison, the GWAS of 93 million imputed variants took 1,175 CPU hours on the same computing node for each anthropometric trait. **Table 1** shows that IBD mapping identified 1,211 association signals outside of any significant GWAS hits. It also shows that many significant 1 cM windows in FiMAP results had at least one imputed tag variant with MAF ≥ 0.01%, imputation quality score ≥ 0.3, and GWAS p-value < 5×10^{-8} in the ± 1 cM flanking regions (total length 3 cM), especially for highly polygenic traits such as standing height and sitting height. Interestingly, the majority of 1 cM windows remained significant even after conditioning on all independent tag variants with GWAS p-value < 5×10^{-8} in each 3 cM region, suggesting that IBD mapping provided complementary association evidence missed by a traditional GWAS approach. **Figure 5** shows that for windows with a significant unconditional FiMAP p-value, conditional p-values were generally larger (less significant) than unconditional p-values as expected, for all 6 anthropometric traits. Of note, we identified a 4 cM region (68 - 72 cM) on chromosome 8 (8q12.1) associated with all 4 anthropometric traits related to body fat distribution or weight (**Figure 6**, minimum p values after conditioning on all independent tag variants: waist circumference 1.2×10^{-10}, hip circumference 2.2×10^{-8}, body mass index 1.7×10^{-10}, body weight 2.1×10^{-10}).

As both RaPID and FiMAP rely on random algorithms, we also used a different random number seed in RaPID IBD segment calling, as well as FiMAP IBD mapping, to investigate the

numerical stability of our findings. **Figure S1** and **Figure S2** show that FiMAP p values were highly stable with respect to different random number seeds used in IBD segment calling (minimum Spearman's $\rho = 0.964$) and IBD mapping (minimum Spearman's $\rho = 0.989$). Moreover, if we had used a one order of magnitude more stringent significance level in FiMAP ($p < 1.47 \times 10^{-6}$), then most significant findings would also pass the Bonferroni-corrected threshold of 1.47×10^{-5} in a separate run with a different random number seed, suggesting that our top findings were robust against different random number seeds used in IBD segment calling and/or IBD mapping.

Discussion

In this work, we have developed FiMAP to conduct fast IBD mapping analysis that scales linearly with the sample size and applied it to the UK Biobank data. Compared to traditional GWAS approaches and variant set tests for sequencing data that utilize only unphased genotypes, IBD mapping with the phase information offers a distinct perspective into the genetic architecture of complex traits by leveraging the genotype similarity in a specific genomic region. The heuristics that if a genomic region is associated with a complex trait, then individuals with greater genotype similarity are also expected to show greater phenotype similarity, have led to the development of linkage analysis methods for family data, including the variance component linkage analysis. However, such methods have not previously been widely applied to biobank-scale population-based cohorts, due to computational challenges.

FiMAP is an accurate and computationally efficient IBD mapping method. It leverages a random matrix to approximate the null distribution of the variance component test statistic in quadratic form. We have found in the UK Biobank data analysis that different random number seeds used in either IBD segment calling by RaPID or IBD mapping by FiMAP had minimal impact on the

top association findings, as the p values were highly consistent regardless of the different random number seeds.

Our simulation studies showed that FiMAP is often more powerful using IBD segments with shorter length cutoffs. However, there is also a tradeoff between statistical power and computational efficiency. With an IBD length cutoff of 10 cM, FiMAP was very computationally efficient, but also had the lowest power in our simulation settings. With an IBD length cutoff of 3 cM, FiMAP was often more powerful than using cutoffs of 5 cM and 10 cM, but the run time also dramatically increased. With even shorter IBD length cutoffs, a much larger number of IBD segments are expected to be called (see Equation 14 of Palamara *et al.*),[5] which may decrease the sparsity of local IBD matrices and lead to a substantial increase in both the run time and memory footprint. In our real data analysis, we chose an IBD length of 5 cM to balance between power and computational efficiency.

In general, the power of IBD mapping depends on the number of IBD segments each sample has in a particular genomic window, which grows quadratically with N. For example, with an IBD length cutoff of 5 cM, the median number of IBD segments per individual per tested window was 17.5 in the full sample (N = 487,279), compared to 0.037 in a random subset of N = 1,000 individuals. Therefore, we expect FiMAP to have much greater statistical power in biobank-scale cohorts, although the actual power may depend on other factors such as the genetic architecture of the trait, as well as the degree of relatedness in the samples. On the other hand, when N is much larger than the size of UK Biobank (in a somewhat distant future), the local IBD matrix may not be sparse enough and new method than FiMAP may be needed for efficient IBD mapping.

Surprisingly, asymptotic p values from FiMAP are not well calibrated even with the sample sizes of the UK Biobank. Although the $N \times N$ local IBD matrices are large in biobank-scale cohorts, they are often sparse with $O(N)$ non-zero off-diagonal elements. As a result, the asymptotic p

values from FiMAP are extremely conservative in the tail. In contrast, our simulation studies under the null hypothesis of no genetic association showed that finite-sample FiMAP p values followed a uniform distribution, after accounting for the variability in estimating the residual variance parameter. Therefore, we recommend the use of finite-sample FiMAP p values for all analyses.

Our UK Biobank anthropometric traits analysis identified a 4 cM region (68 - 72 cM) on chromosome 8 (8q12.1) associated with all 4 anthropometric traits related to body fat distribution or weight. Although previous studies have reported associations with BMI[49-53] in this region (minimum GWAS p-value 1×10^{-14}),[51] as well as BMI-adjusted waist circumference (minimum GWAS p-value 4×10^{-11})[50] and hip circumference (minimum GWAS p-value 9×10^{-10})[54] in ± 1 Mb nearby regions, they were not among the best known associations from GWAS for these phenotypes. Moreover, there were no known GWAS associations for body weight in this region. Genes in this region include *UBXN2B* (an adapter protein required for Golgi and endoplasmic reticulum biogenesis)[55] and *CYP7A1* (a cytochrome P450 monooxygenase involved in drug metabolism and synthesis of cholesterol, steroids and other lipids),[56-60] which may be involved in lipids metabolism and body fat distribution.

FiMAP, or IBD mapping in general, has several advantages compared to traditional GWAS approaches and variant set tests on unphased genotypes. It may better tag rare causal variants, especially when they are not directly genotyped, which is often the case for commonly used genotyping arrays. Although it is unlikely that rare causal variants are not genotyped using the whole genome sequencing technology, as the RaPID algorithm tolerates mismatches, FiMAP is more robust to genotyping or sequencing errors since each individual genetic variant would not dramatically change the IBD segment calling. Moreover, the phasing information is usually ignored in traditional GWAS approaches and variant set tests, and our simulation studies showed that FiMAP is more powerful in identifying the genetic association in the case of

haplotype effects. Our conditional analysis for UK Biobank anthropometric traits showed that most 1 cM windows identified by FiMAP remained significant after adjusting for all GWAS tag variants in the window and flanking regions, suggesting that these associations could not be fully explained by unphased genotypes and haplotype effects might play an important role in the genetic architecture of complex traits.

FiMAP also has a few limitations. It tests a few thousand 1 cM windows on the human genome, and therefore requires a much less stringent significance level than traditional GWAS approaches which test millions of genetic variants. However, the major limitation of FiMAP is the low resolution of association signals. Follow-up analysis is often needed to identify causal variants or interpret these association findings. For example, we can shorten the window size from 1 cM to the size of genes, and conduct gene-based IBD mapping tests using local IBD matrices defined on each gene and flanking regions. Also, currently FiMAP can only be applied to quantitative traits in a linear mixed model framework, and future work includes extension to binary traits using logistic mixed models, as well as survival traits using Cox mixed models. Nevertheless, FiMAP empowers computationally efficient IBD mapping for complex traits using variance component linkage analysis models with unprecedented sample sizes from biobank-scale cohorts.

Supplemental Data

Supplemental Data include 2 figures.

Declaration of Interests

The authors declare no competing interests.

Acknowledgments

This work was supported by National Institutes of Health grants R00 HL130593 (to H.C.) and R01 HG010086 (to A.N. and D.Z.). This research has been conducted using the UK Biobank Resource under Application Number 24247.

Web Resources

The URLs for data presented herein are as follows.

FiMAP, https://github.com/hanchenphd/FiMAP

GMMAT, https://github.com/hanchenphd/GMMAT

RaPID, https://github.com/ZhiGroup/RaPID

References

1. Thompson, E.A. (2013). Identity by descent: variation in meiosis, across genomes, and in populations. Genetics 194, 301-326.

2. Balding, D.J., Nichols, R.A. (1994). DNA profile match probability calculation: how to allow for population stratification, relatedness, database selection and single bands. Forensic Sci. Int. 64, 125-140.

3. Kling, D., Tillmar, A. (2019). Forensic genealogy-A comparison of methods to infer distant relationships based on dense SNP data. Forensic. Sci. Int. Genet. 42, 113-124.

4. Albrechtsen, A., Moltke, I., Nielsen, R. (2010). Natural selection and the distribution of identity-by-descent in the human genome. Genetics 186, 295-308.

5. Palamara, P.F., Lencz, T., Darvasi, A., Pe'er, I. (2012). Length distributions of identity by descent reveal fine-scale demographic history. Am. J. Hum. Genet. 91, 809-822.

6. Han, L., Abney, M. (2013). Using identity by descent estimation with dense genotype data to detect positive selection. Eur. J. Hum. Genet. 21, 205-211.

7. Ramstetter, M.D., Shenoy, S.A., Dyer, T.D., Lehman, D.M., Curran, J.E., Duggirala, R., Blangero, J., Mezey, J.G., Williams, A.L. (2018). Inferring Identical-by-Descent Sharing of Sample Ancestors Promotes High-Resolution Relative Detection. Am. J. Hum. Genet. 103, 30-44.

8. Astle, W., Balding, D.J. (2009). Population Structure and Cryptic Relatedness in Genetic Association Studies. Statistical Science 24, 451-471.

9. Thornton, T.A. (2015). Statistical methods for genome-wide and sequencing association studies of complex traits in related samples. Curr. Protoc. Hum. Genet. 84, 1.28.1-1.28.9.

10. Wang, B., Sverdlov, S., Thompson, E. (2017). Efficient Estimation of Realized Kinship from Single Nucleotide Polymorphism Genotypes. Genetics 205, 1063-1078.

11. Naseri, A., Shi, J., Lin, X., Zhang, S., Zhi, D. (2021). RAFFI: Accurate and fast familial relationship inference in large scale biobank studies using RaPID. PLoS Genet. 17, e1009315.

12. Goldgar, D.E. (1990). Multipoint analysis of human quantitative genetic variation. Am. J. Hum. Genet. 47, 957-967.

13. Amos, C.I. (1994). Robust variance-components approach for assessing genetic linkage in pedigrees. Am. J. Hum. Genet. 54, 535-543.

14. Xu, S., Atchley, W.R. (1995). A random model approach to interval mapping of quantitative trait loci. Genetics 141, 1189-1197.

15. Almasy, L., Blangero, J. (1998). Multipoint quantitative-trait linkage analysis in general pedigrees. Am. J. Hum. Genet. 62, 1198-1211.

16. Houwen, R.H., Baharloo, S., Blankenship, K., Raeymaekers, P., Juyn, J., Sandkuijl, L.A., Freimer, N.B. (1994). Genome screening by searching for shared segments: mapping a gene for benign recurrent intrahepatic cholestasis. Nat. Genet. 8, 380-386.

17. Gusev, A., Kenny, E.E., Lowe, J.K., Salit, J., Saxena, R., Kathiresan, S., Altshuler, D.M., Friedman, J.M., Breslow, J.L., Pe'er, I. (2011). DASH: a method for identical-by-descent haplotype mapping uncovers association with recent variation. Am. J. Hum. Genet. 88, 706-717.

18. Browning, S.R., Thompson, E.A. (2012). Detecting rare variant associations by identity-by-descent mapping in case-control studies. Genetics 190, 1521-1531.

19. Vacic, V., Ozelius, L.J., Clark, L.N., Bar-Shira, A., Gana-Weisz, M., Gurevich, T., Gusev, A., Kedmi, M., Kenny, E.E., Liu, X. et al. (2014). Genome-wide mapping of IBD segments in an Ashkenazi PD cohort identifies associated haplotypes. Hum. Mol. Genet. 23, 4693-4702.

20. Hsueh, W.C., Nair, A.K., Kobes, S., Chen, P., Goring, H.H.H., Pollin, T.I., Malhotra, A., Knowler, W.C., Baier, L.J., Hanson, R.L. (2017). Identity-by-Descent Mapping Identifies Major

Locus for Serum Triglycerides in Amerindians Largely Explained by an APOC3 Founder Mutation. Circ. Cardiovasc. Genet. 10, 10.1161/CIRCGENETICS.117.001809.

21. Westerlind, H., Imrell, K., Ramanujam, R., Myhr, K.M., Celius, E.G., Harbo, H.F., Oturai, A.B., Hamsten, A., Alfredsson, L., Olsson, T. et al. (2015). Identity-by-descent mapping in a Scandinavian multiple sclerosis cohort. Eur. J. Hum. Genet. 23, 688-692.

22. Henden, L., Twine, N.A., Szul, P., McCann, E.P., Nicholson, G.A., Rowe, D.B., Kiernan, M.C., Bauer, D.C., Blair, I.P., Williams, K.L. (2020). Identity by descent analysis identifies founder events and links SOD1 familial and sporadic ALS cases. NPJ Genom. Med. 5, 32-8. eCollection 2020.

23. Morgenthaler, S., Thilly, W.G. (2007). A strategy to discover genes that carry multi-allelic or mono-allelic risk for common diseases: a cohort allelic sums test (CAST). Mutat. Res. 615, 28-56.

24. Li, B., Leal, S.M. (2008). Methods for detecting associations with rare variants for common diseases: application to analysis of sequence data. Am. J. Hum. Genet. 83, 311-321.

25. Madsen, B.E., Browning, S.R. (2009). A groupwise association test for rare mutations using a weighted sum statistic. PLoS Genet. 5, e1000384.

26. Morris, A.P., Zeggini, E. (2010). An evaluation of statistical approaches to rare variant analysis in genetic association studies. Genet. Epidemiol. 34, 188-193.

27. Wu, M.C., Lee, S., Cai, T., Li, Y., Boehnke, M., Lin, X. (2011). Rare-variant association testing for sequencing data with the sequence kernel association test. Am. J. Hum. Genet. 89, 82-93.

28. Lee, S., Wu, M.C., Lin, X. (2012). Optimal tests for rare variant effects in sequencing association studies. Biostatistics 13, 762-775.

29. Sun, J., Zheng, Y., Hsu, L. (2013). A unified mixed-effects model for rare-variant association in sequencing studies. Genet. Epidemiol. 37, 334-344.

30. Loh, P.R., Palamara, P.F., Price, A.L. (2016). Fast and accurate long-range phasing in a UK Biobank cohort. Nat. Genet. 48, 811-816.

31. Loh, P.R., Danecek, P., Palamara, P.F., Fuchsberger, C., A Reshef, Y., K Finucane, H., Schoenherr, S., Forer, L., McCarthy, S., Abecasis, G.R. et al. (2016). Reference-based phasing using the Haplotype Reference Consortium panel. Nat. Genet. 48, 1443-1448.

32. Delaneau, O., Zagury, J.F., Robinson, M.R., Marchini, J.L., Dermitzakis, E.T. (2019). Accurate, scalable and integrative haplotype estimation. Nat. Commun. 10, 5436-y.

33. Naseri, A., Tang, K., Geng, X., Shi, J., Zhang, J., Shakya, P., Liu, X., Zhang, S., Zhi, D. (2021). Personalized genealogical history of UK individuals inferred from biobank-scale IBD segments. BMC Biol. 19, 32-y.

34. Durbin, R. (2014). Efficient haplotype matching and storage using the positional Burrows-Wheeler transform (PBWT). Bioinformatics 30, 1266-1272.

35. Naseri, A., Liu, X., Tang, K., Zhang, S., Zhi, D. (2019). RaPID: ultra-fast, powerful, and accurate detection of segments identical by descent (IBD) in biobank-scale cohorts. Genome Biol. 20, 143-8.

36. Zhou, Y., Browning, S.R., Browning, B.L. (2020). A Fast and Simple Method for Detecting Identity-by-Descent Segments in Large-Scale Data. Am. J. Hum. Genet. 106, 426-437.

37. Freyman, W.A., McManus, K.F., Shringarpure, S.S., Jewett, E.M., Bryc, K., 23 and Me Research Team, Auton, A. (2021). Fast and Robust Identity-by-Descent Inference with the Templated Positional Burrows-Wheeler Transform. Mol. Biol. Evol. 38, 2131-2151.

38. Nait Saada, J., Kalantzis, G., Shyr, D., Cooper, F., Robinson, M., Gusev, A., Palamara, P.F. (2020). Identity-by-descent detection across 487,409 British samples reveals fine scale population structure and ultra-rare variant associations. Nat. Commun. 11, 6130-x.

39. Shemirani, R., Belbin, G.M., Avery, C.L., Kenny, E.E., Gignoux, C.R., Ambite, J.L. (2019). Rapid detection of identity-by-descent tracts for mega-scale datasets. bioRxiv, 749507.

40. Liu, D., Lin, X., Ghosh, D. (2007). Semiparametric regression of multidimensional genetic pathway data: least-squares kernel machines and linear mixed models. Biometrics 63, 1079-1088.

41. Kwee, L.C., Liu, D., Lin, X., Ghosh, D., Epstein, M.P. (2008). A powerful and flexible multilocus association test for quantitative traits. Am. J. Hum. Genet. 82, 386-397.

42. Chen, H., Wang, C., Conomos, M.P., Stilp, A.M., Li, Z., Sofer, T., Szpiro, A.A., Chen, W., Brehm, J.M., Celedon, J.C. et al. (2016). Control for Population Structure and Relatedness for Binary Traits in Genetic Association Studies via Logistic Mixed Models. Am. J. Hum. Genet. 98, 653-666.

43. Chen, J., Chen, W., Zhao, N., Wu, M.C., Schaid, D.J. (2016). Small Sample Kernel Association Tests for Human Genetic and Microbiome Association Studies. Genet. Epidemiol. 40, 5-19.

44. Zhan, X., Xue, L., Zheng, H., Plantinga, A., Wu, M.C., Schaid, D.J., Zhao, N., Chen, J. (2018). A small-sample kernel association test for correlated data with application to microbiome association studies. Genet. Epidemiol. 42, 772-782.

45. Zhai, J., Knox, K., Twigg, H.L., Zhou, H., Zhou, J.J. (2019). Exact variance component tests for longitudinal microbiome studies. Genet. Epidemiol. 43, 250-262.

46. Chen, H., Huffman, J.E., Brody, J.A., Wang, C., Lee, S., Li, Z., Gogarten, S.M., Sofer, T., Bielak, L.F., Bis, J.C. et al. (2019). Efficient Variant Set Mixed Model Association Tests for Continuous and Binary Traits in Large-Scale Whole-Genome Sequencing Studies. Am. J. Hum. Genet. 104, 260-274.

47. Naseri, A., Zhi, D., Zhang, S. (2020). Discovery of runs-of-homozygosity diplotype clusters and their associations with diseases in UK Biobank. medRxiv.

48. Sofer, T., Zheng, X., Gogarten, S.M., Laurie, C.A., Grinde, K., Shaffer, J.R., Shungin, D., O'Connell, J.R., Durazo-Arvizo, R.A., Raffield, L. et al. (2019). A fully adjusted two-stage procedure for rank-normalization in genetic association studies. Genet. Epidemiol.

49. Kichaev, G., Bhatia, G., Loh, P.R., Gazal, S., Burch, K., Freund, M.K., Schoech, A., Pasaniuc, B., Price, A.L. (2019). Leveraging Polygenic Functional Enrichment to Improve GWAS Power. Am. J. Hum. Genet. 104, 65-75.

50. Zhu, Z., Guo, Y., Shi, H., Liu, C.L., Panganiban, R.A., Chung, W., O'Connor, L.J., Himes, B.E., Gazal, S., Hasegawa, K. et al. (2020). Shared genetic and experimental links between obesity-related traits and asthma subtypes in UK Biobank. J. Allergy Clin. Immunol. 145, 537-549.

51. Hoffmann, T.J., Choquet, H., Yin, J., Banda, Y., Kvale, M.N., Glymour, M., Schaefer, C., Risch, N., Jorgenson, E. (2018). A Large Multiethnic Genome-Wide Association Study of Adult Body Mass Index Identifies Novel Loci. Genetics 210, 499-515.

52. Pulit, S.L., Stoneman, C., Morris, A.P., Wood, A.R., Glastonbury, C.A., Tyrrell, J., Yengo, L., Ferreira, T., Marouli, E., Ji, Y. et al. (2019). Meta-analysis of genome-wide association studies for body fat distribution in 694 649 individuals of European ancestry. Hum. Mol. Genet. 28, 166-174.

53. Akiyama, M., Okada, Y., Kanai, M., Takahashi, A., Momozawa, Y., Ikeda, M., Iwata, N., Ikegawa, S., Hirata, M., Matsuda, K. et al. (2017). Genome-wide association study identifies 112 new loci for body mass index in the Japanese population. Nat. Genet. 49, 1458-1467.

54. Shungin, D., Winkler, T.W., Croteau-Chonka, D.C., Ferreira, T., Locke, A.E., Magi, R., Strawbridge, R.J., Pers, T.H., Fischer, K., Justice, A.E. et al. (2015). New genetic loci link adipose and insulin biology to body fat distribution. Nature 518, 187-196.

55. Uchiyama, K., Totsukawa, G., Puhka, M., Kaneko, Y., Jokitalo, E., Dreveny, I., Beuron, F., Zhang, X., Freemont, P., Kondo, H. (2006). p37 is a p97 adaptor required for Golgi and ER biogenesis in interphase and at the end of mitosis. Dev. Cell. 11, 803-816.

56. Norlin, M., Toll, A., Bjorkhem, I., Wikvall, K. (2000). 24-hydroxycholesterol is a substrate for hepatic cholesterol 7alpha-hydroxylase (CYP7A). J. Lipid Res. 41, 1629-1639.

57. Bodin, K., Andersson, U., Rystedt, E., Ellis, E., Norlin, M., Pikuleva, I., Eggertsen, G., Bjorkhem, I., Diczfalusy, U. (2002). Metabolism of 4 beta -hydroxycholesterol in humans. J. Biol. Chem. 277, 31534-31540.

58. Li, T., Chanda, D., Zhang, Y., Choi, H.S., Chiang, J.Y. (2010). Glucose stimulates cholesterol 7alpha-hydroxylase gene transcription in human hepatocytes. J. Lipid Res. 51, 832-842.

59. Noshiro, M., Okuda, K. (1990). Molecular cloning and sequence analysis of cDNA encoding human cholesterol 7 alpha-hydroxylase. FEBS Lett. 268, 137-140.

60. Shinkyo, R., Xu, L., Tallman, K.A., Cheng, Q., Porter, N.A., Guengerich, F.P. (2011). Conversion of 7-dehydrocholesterol to 7-ketocholesterol is catalyzed by human cytochrome P450 7A1 and occurs by direct oxidation without an epoxide intermediate. J. Biol. Chem. 286, 33021-33028.

Tables

Table 1. Numbers of significant 1 cM windows in UK Biobank IBD mapping and conditional analyses for 6 anthropometric traits. Statistical significance was defined as p value < 1.47×10^{-5} for FiMAP, and single-variant test p value < 5×10^{-8} for GWAS. Overlapping with GWAS hits was defined as a significant 1 cM unconditional FiMAP test region with at least one imputed tag variant with MAF ≥ 0.01%, imputation quality score ≥ 0.3, and GWAS p-value < 5×10^{-8} in the ± 1 cM flanking regions (total length of 3 cM). Conditional FiMAP tests were performed after adjusting for independent tag variants in each 3 cM region from GWAS.

Trait	Unconditional	Overlapping GWAS	Conditional
Waist circumference	140	79 (56%)	116 (83%)
Hip circumference	60	41 (68%)	44 (73%)
Standing height	2,416	1,663 (69%)	2,282 (94%)
Sitting height	1,033	750 (73%)	819 (79%)
Body mass index	219	136 (62%)	166 (76%)
Body weight	70	58 (83%)	41 (59%)

Figures

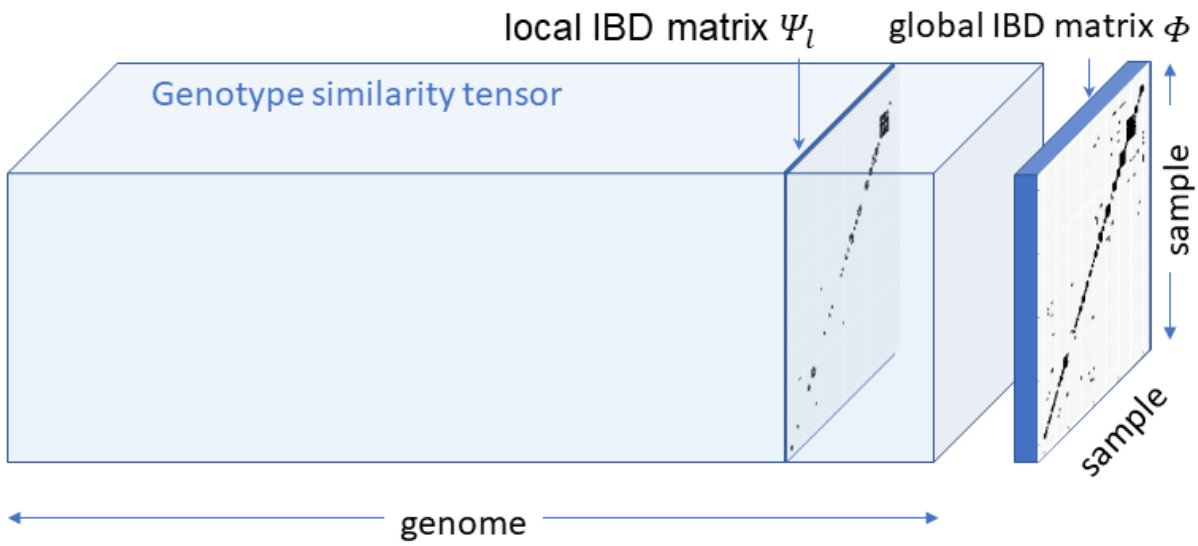

Figure 1. Local and global IBD matrices in FiMAP. The global IBD matrix Φ is the average of the local IBD matrices Ψ_l along the genome dimension of the genotype similarity tensor.

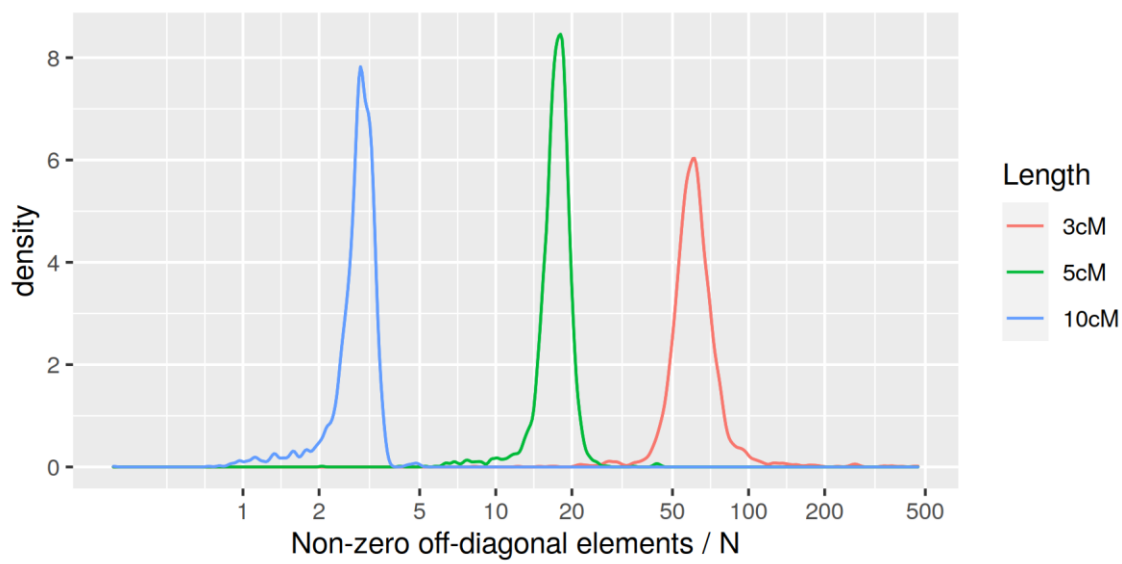

Figure 2. Distribution of non-zero off-diagonal elements in local IBD matrices. For each color, a total of 3,403 local IBD matrices of sample size N = 487,279 for 1 cM windows were

plotted. The local IBD matrices were constructed from RaPID IBD segments called with length ≥ 3 cM, 5 cM, 10 cM.

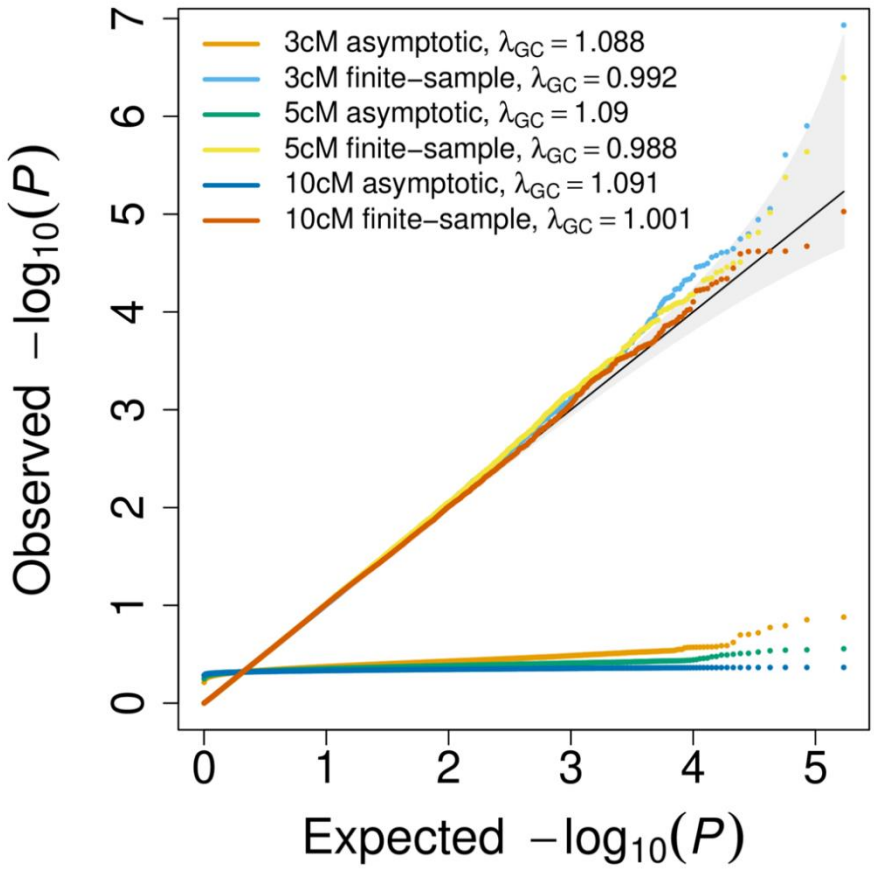

Figure 3. Quantile-quantile plot of asymptotic and finite-sample FiMAP p values under the null hypothesis. A total of 170,150 p values from 50 simulation replicates were plotted. The genomic inflation factor λ_{GC} was computed using the observed median p values. The local IBD matrices were constructed from RaPID IBD segments called with length ≥ 3 cM, 5 cM, 10 cM.

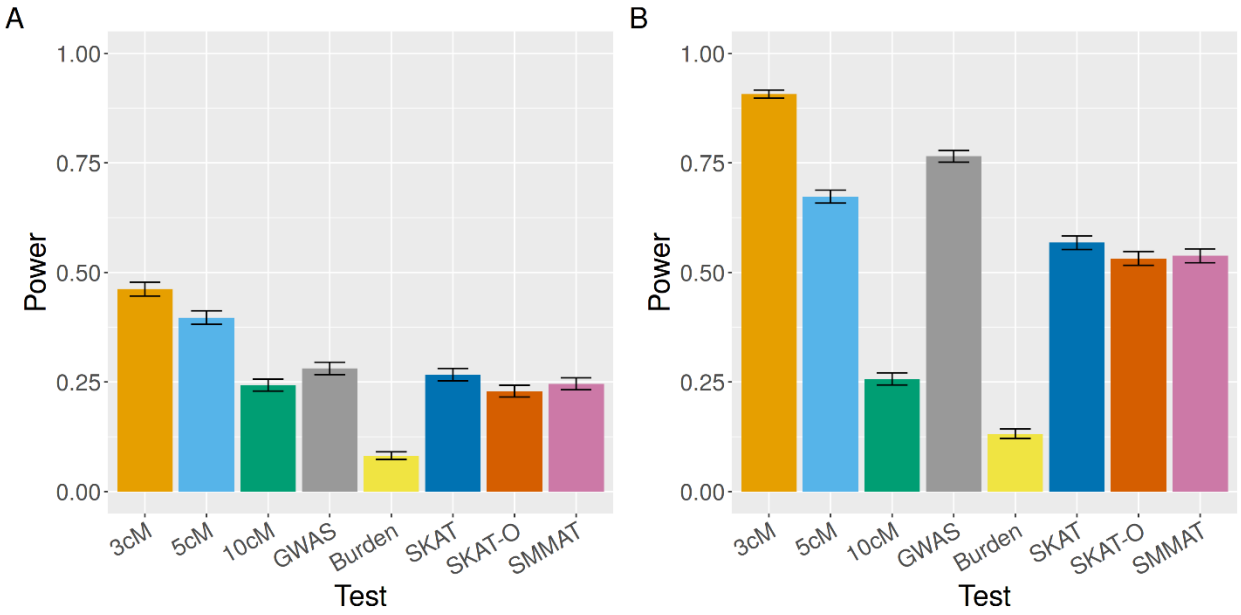

Figure 4. Power comparison of FiMAP, GWAS and variant set tests. (A) Untyped rare causal variants; (B) Causal haplotype effects. In each simulation replicate with 1 cM window, finite-sample FiMAP with local IBD matrices constructed from RaPID IBD segments called with length ≥ 3 cM, 5 cM, 10 cM were benchmarked with a GWAS single-variant test with a Bonferroni correction for the minimum p value, and four variant set tests on the same window: the burden test, SKAT, SKAT-O and SMMAT. Empirical power was estimated as the proportion of p values less than 0.05 over 1,000 simulation replicates.

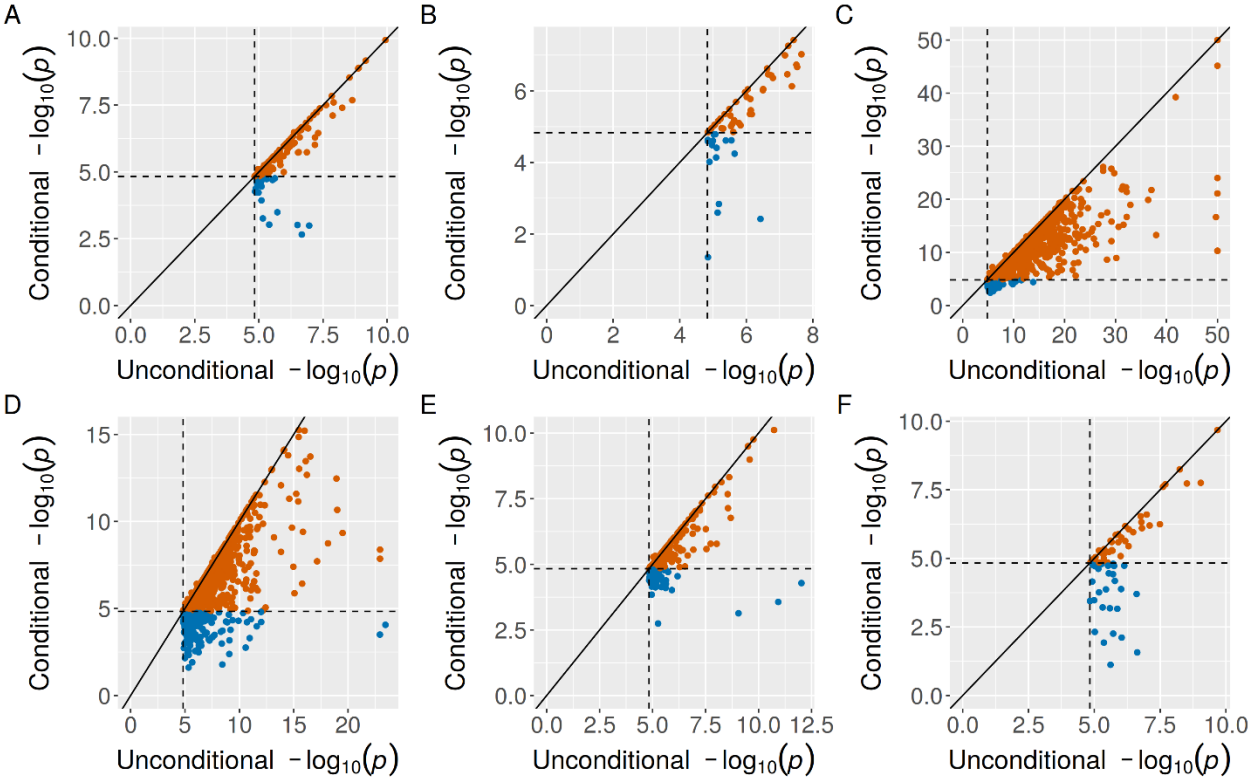

Figure 5. Comparison of IBD mapping p values before and after conditioning on significant tag variants in the testing window and flanking regions. (A) Waist circumference; (B) Hip circumference; (C) Standing height; (D) Sitting height; (E) Body mass index; (F) Body weight. Dashed lines represented the Bonferroni-corrected significance level of 0.05/3,403 = 1.47×10^{-5}. Only significant unconditional FiMAP p values were shown. P values < 1×10^{-50} for standing height were truncated at 1×10^{-50}. FiMAP conditional p-values that no longer reach significance were shown in blue.

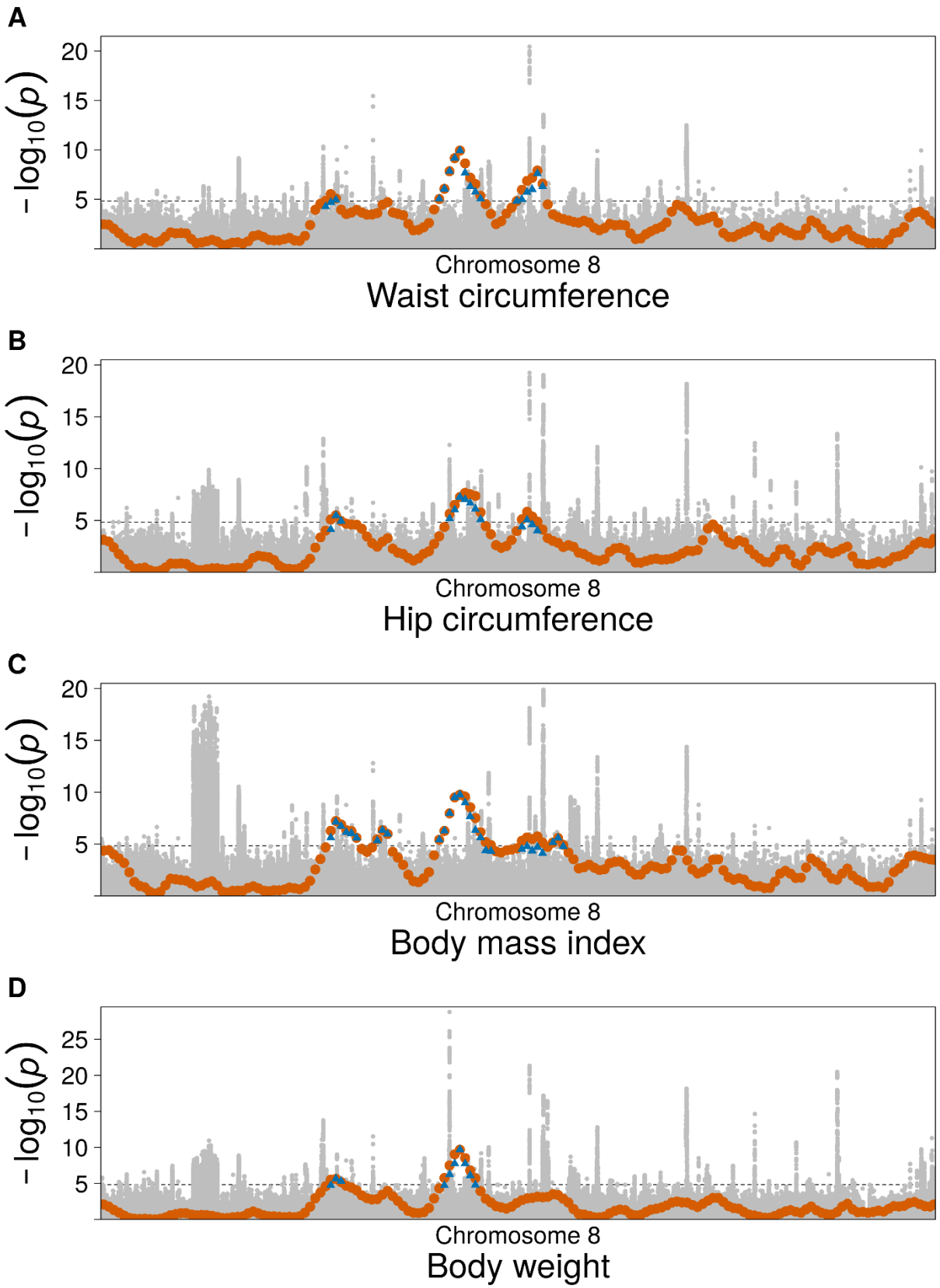
A
20
15
10
5
$-\log_{10}(p)$
Chromosome 8
Waist circumference
B
20
15
10
5
$-\log_{10}(p)$
Chromosome 8
Hip circumference
C
20
15
10
5
$-\log_{10}(p)$
Chromosome 8
Body mass index
D
25
20
15
10
5
$-\log_{10}(p)$
Chromosome 8
Body weight

Figure 6. GWAS and FiMAP p values on chromosome 8. (A) Waist circumference; (B) Hip circumference; (C) Body mass index; (D) Body weight. GWAS p values were shown in grey and unconditional FiMAP p values were shown in orange. For windows with unconditional FiMAP p values $< 1.47 \times 10^{-5}$, conditional p values after adjusting for all independent GWAS tag variants were shown in blue triangles.